J. Fluid Mech. (1983), *vol.* 135, *pp.* 27–50
Printed in Great Britain

On solitary waves running down an inclined plane

By A. PUMIR, P. MANNEVILLE† AND Y. POMEAU
Division de la physique, CEN-Saclay, 91191 Gif-sur-Yvette, France

(Received 16 August 1982 and in revised form 12 May 1983)

We study the existence and the role of solitary waves in the instability of a fluid layer flowing down an inclined plane. The approach presented is fully nonlinear. Solitary waves steady in a moving frame are described by homoclinic trajectories of an associated ordinary differential equation. They are searched numerically for a given value of viscosity and surface tension. Several kinds of solitary waves can exist, characterized by their number n of humps. We investigate the stability of these waves by integrating the initial-value problem directly. Solitary waves with more than 1 hump did not appear in the simulation, and moreover a catastrophic behaviour took place for too large a Reynolds number ($R \gtrsim R_1^*$) or too large an amplitude, suggesting a finite-time singularity. The long-term evolution is shown to be a very slow relaxation to a steady state in a moving frame. The relation to the experimental observation of localized wavetrains is also discussed.

1. Introduction

Theoretical understanding of the nonlinear development of instability and transition to turbulence in parallel flows is commonly believed to be less advanced than in the case of Rayleigh–Bénard convection for instance (see e.g. Swinney & Gollub 1981).

In parallel flows the perturbative approach in terms of normal modes does not take account of strongly nonlinear localized structures, which seem to play an important role in the transition process (see Tritton 1977). In order to attack this problem, we have considered the 'simple' case of the instability of a liquid layer flowing down an inclined plate. Kapitza & Kapitza (1949) studied experimentally the related problem of a liquid layer flowing down a vertical cylinder. Several regimes involving solitary waves were observed. The analysis of such solutions is difficult to understand within the framework of standard normal-mode analysis and perturbation theory. In the words of Kapitza & Kapitza:

'A quantitative description of the properties of the single waves of a thin fluid flow layer in the presence of viscosity and surface tension will obviously be associated with such serious mathematical difficulties that one can scarcely expect to overcome them.'

Benjamin (1957) and Yih (1963) solved the linear stability problem for the basic flow of constant thickness and determined the critical Reynolds number R_c for instability. The subsequent analysis of the weakly nonlinear evolution relied mostly on a Landau-equation formalism (Landau & Lifshitz 1959*a*). Benney (1966) derived an equation of the form

$$\frac{\mathrm{d}}{\mathrm{d}t}|a|^2 = \eta|a|^2 - \gamma|a|^4, \tag{1}$$

† Permanent address: DPh-G/PRSM, Orme des Merisiers 91191 Gif-sur-Yvette, France.

where η is small and proportional to $R-R_c$ near R_c. Later Lin (1969) and Gjevik (1970), taking superficial tension into account, showed that the amplitude $|a|$ of spatially periodic perturbations tends to a small but finite value for $R \to R_c$, i.e. $\gamma > 0$.

Lin (1974) derived an equation for the envelope function describing a slowly modulated periodic solution. Nakaya (1975) improved the nonlinear analysis and also found a supercritical or normal bifurcation. More recently, Sivashinsky & Michelson (1980) and Sivashinsky & Schlang (1982) studied the limit of large superficial tension and obtained a simple nonlinear partial differential equation known for having a spontaneously turbulent solution. We begin this paper with a short presentation of the partial differential equation which governs the height of the flowing film made of Newtonian viscous fluid, and discuss briefly the linear stability problem, defining the relevant critical Reynolds number R_c (§2). But we are mostly interested in finite-amplitude localized solutions, and turn to the problem of 'solitary waves'. The possibility of such solutions was pointed out by Benney (1966) on the basis of an analogy with the Korteweg–de Vries equation in the weakly nonlinear limit. Here we do not restrict ourselves to weak nonlinearities, and we look for 'solitary waves' (§3). These waves are assumed to travel without deformation in a frame moving at a certain velocity v relative to the laboratory frame. In terms of the moving coordinate, they are governed by an ordinary differential equation. Both upstream and downstream the height of the perturbed film tends to the unperturbed height of the basic flow. In the theory of dynamical systems, such solutions are called homoclinic trajectories (see e.g. Smale 1967). These special solutions exist only for special values of the velocity v at given Reynolds number. This relation $v(R)$ is determined numerically for the different kinds of solitary waves which can appear with $1, 2, \ldots$ principal humps. The stability (i.e. the actual existence) of these solutions is not obvious. Thus in order to ascertain it, we have investigated the initial-value problem for the complete partial differential equation (§4). In our simulations only one kind of solitary waves could be observed, namely those with only one hump. In some cases the evolution was quite complicated, looking turbulent, but we have some evidence that this behaviour was only transient. We shall also report on other cases where a catastrophic evolution suggests a breaking of the film. Finally we discuss the relevance of ideas and methods developed in this paper for the more general case of localized structures in parallel flows to which we have alluded at the beginning.

2. Fundamental equations and the linear stability problem

Kapitza & Kapitza (1949) studied experimentally a thin film of liquid flowing down a vertical cylinder. The case of an inclined plate is slightly different since curvature effects disappear, while the inclination angle introduces itself as a new parameter controlling the instability threshold. Here we consider a film of viscous fluid flowing down a plane under the action of gravity. This situation is pictured in figure 1. We take the x- and z-axes in the plane, x being in the direction of largest slope. The y-axis is perpendicular to the plane. In what follows we consider 2-dimensional flows only; that is to say flows parallel to the (x, y)-plane and independent of the transverse coordinate z. We shall reconsider this important restriction later. Let $h(x, t)$ be the ordinate of the free surface of the fluid layer at abscissa x and time t and

$$Q(x,t) = \int_0^{h(x,t)} \mathrm{d}y\, u(x,y,t)$$

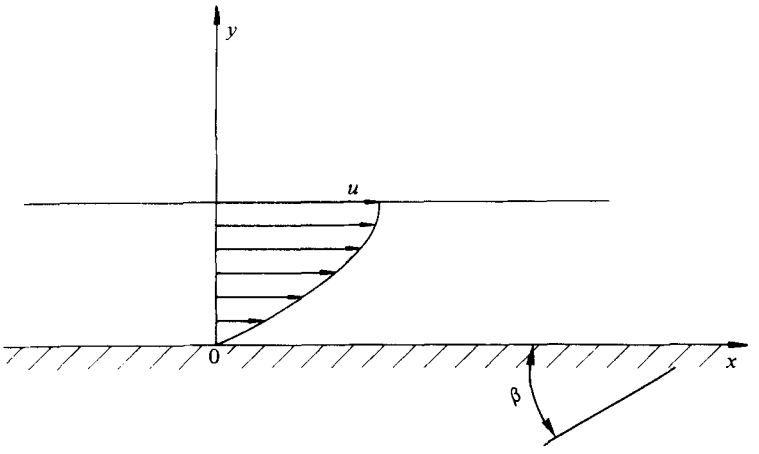

FIGURE 1. Velocity profile of the basic flow on a plate inclined with respect to the horizontal in the presence of gravity.

be the flow rate parallel to the direction of the largest slope (x). The incompressibility condition and the kinematics of the free surface lead to the equation

$$h_t + Q_x = 0. \tag{2}$$

Indices x and t denote partial derivatives. The flow rate Q can be expressed as a function of h by using the Navier–Stokes equations in the long-wave limit, that is when the range of variation of h as a function of t is much larger than the layer thickness. Following Kapitza, who interpreted his observations as the result of combined effects of gravity and surface tension, we assume that $W\alpha^2 \sim 1$ and $\alpha^{-1} \gg 1$, where $\alpha = h_0/l$ is the (small) ratio of the undisturbed layer thickness h_0 to the lengthscale l for x-variations and where W is the Weber number comparing gravity forces to surface tension. Thus, retaining terms up to order α and $W\alpha^3$ included in the expression of Q, one obtains (Lin 1974; Nakaya 1975) from (2)

$$h_t + (\tfrac{2}{3}h^3 + (\tfrac{8}{15}Rh^6 - \tfrac{2}{3}Bh^3)\,h_x + \tfrac{2}{3}Wh^3h_{xxx})_x = 0, \tag{3}$$

where R is the Reynolds number of the undisturbed flow and B is the cotangent of the angle between the horizontal direction and the x-axis. The unit length in (3) is the thickness of the undisturbed film.

The main reason to believe that (3) is a consistent approximation is the following. Let us consider the stability of the basic flow ($h = 1$) against infinitesimal perturbations. Writing $h = 1 + \delta h$, upon linearization of (3) we get

$$\delta h_t + 2\delta h_x + (\tfrac{8}{15}R - \tfrac{2}{3}B)\,\delta h_{xx} + \tfrac{2}{3}W\delta h_{xxxx} = 0, \tag{4}$$

and look for solutions of the form $\delta h = H\exp(iqx + \sigma t)$. Equation (4) leads to

$$\sigma + 2iq - (\tfrac{8}{15}R - \tfrac{2}{3}B)\,q^2 + \tfrac{2}{3}Wq^4 = 0,$$

or

$$\mathrm{Re}\,(\sigma) = (\tfrac{8}{15}R - \tfrac{2}{3}B)\,q^2 - \tfrac{2}{3}Wq^4$$

and

$$\mathrm{Im}\,(\sigma) = -2q.$$

For $R < R_c \equiv \frac{5}{4}B$ all infinitesimal perturbations are damped, while for $R > R_c$ there exists a finite band of unstable wavevectors near $q = 0$. As $-\mathrm{Im}(\sigma)/q = 2$ all these wavevectors have the same phase velocity. With our sign convection this is a downstream velocity.

The role of each term in (3) can be understood now as follows. The advection of the free surface is described by $(\frac{2}{3}h^3)_x$, while $((\frac{8}{15}Rh^6 - \frac{2}{3}Bh^3)h_x)_x$ describes the instability of the free surface. The stabilizing effect of surface tension is taken into account by $(\frac{2}{3}Wh^3h_{xxx})_x$, and this term is the first stabilizing one that appears in the long-wavelength expansion. It is necessary in particular to avoid the occurrence of an ill-defined evolution equation unstable for infinitely large wavenumbers. This is true indeed for the linearized equation (4), because, as we shall see in this paper, the nonlinear equation (3) may develop singularities from smooth initial conditions after a finite time.

The equation (3) describes consistently the evolution of the film because it includes all qualitatively important effects at their lowest order in α: nonlinearities, short-wavenumber instability, large-wavenumber stability. In what follows, we shall use dimensionless values of W, R and B, noticeably in our numerical computations.

Nevertheless, our study could be of more general interest, because it retains all qualitatively important effects in the evolution of the instability. As noticed by Lin (1974), the fact that in (3) a band of wavenumbers, including zero, are linearly unstable is appropriate for the description of 'single' or solitary waves.

3. Solitary waves at rest in a moving frame (from the point of view of dynamical system theory)

3.1. *General scope and qualitative aspects of solitary waves*

We look for special solutions of (3) travelling without deformation in a frame moving relative to the laboratory frame at a certain speed v. Then setting $h(x,t) = h(z)$, where $z = x - vt$, and denoting derivatives with respect to z by primes, for such solutions we can write (3) in the form

$$-\tfrac{3}{2}vh' + [h^3 + \tfrac{4}{5}(Rh^6 - R_c h^3)h' + Wh^3h''']' = 0, \tag{5}$$

where $R_c = \frac{5}{4}B$ as shown earlier. Obviously (5) admits a first integral

$$-\tfrac{3}{2}vh + h^3 + \tfrac{4}{5}(Rh^6 - R_c h^3)h' + Wh^3h''' = K. \tag{6}$$

Among the solutions corresponding to a given K we are interested in solitary waves, i.e. localized patterns. Such solutions tend to a constant far from the perturbed region: when z tends to $\pm\infty$ h tends to $h(\pm\infty)$ and h', h'', h''' tend to zero. We shall consider mostly the case $h(+\infty) = h(-\infty) = h_0(= 1)$ for which $K = 1 - \frac{3}{2}v$, but a situation with $h(+\infty) \neq h(-\infty)$ can also be described by (6). It occurs if the flow rate is suddenly increased or decreased ($h(-\infty) > h(+\infty)$ and $h(+\infty) > h(-\infty)$ respectively, since the flow rate is an increasing function of height); in this case the equation $K = h^3 - \frac{3}{2}vh$ must have two real positive roots h_1 and h_2, as it fixes the values of the first integral when $h' = h'' = 0$ far away from the perturbed region. Without loss of generality, one can set $h_1 = 1$, h_2 being larger than 1 if $v > 2$ and smaller in the opposite case.

Since h is the thickness of the fluid film, we are interested in solutions where h is strictly positive everywhere. If h reaches zero somewhere this means that the film

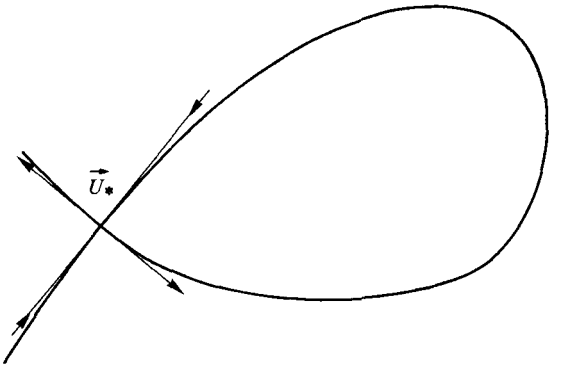

FIGURE 2. An homoclinic trajectory in a 2-dimensional phase space (≡ a plane). In this case the homoclinic curve is also called a separatrix.

is interrupted on contact lines, and (3) loses its meaning. For $h > 0$, (6) can be written in the form of a first-order differential system:

$$U_1' = U_2, \quad U_2' = U_3, \tag{7a, b}$$

$$U_3' = \frac{1}{W}\left[\frac{1-U_1}{U_1^3}(U_1^2+U_1+1-\tfrac{3}{2}v)-\tfrac{4}{5}(RU_1^3-R_c)\,U_2\right], \tag{7c}$$

where $U_1 = h, U_2 = h', U_3 = h''$ using $K = 1-\frac{3}{2}v$. Formally we shall write (7) as

$$\frac{dU}{dz} = F(U), \tag{8}$$

a form which is more appropriate to discuss solutions within the framework of dynamical-system theory. System (7) defines a 'flow' in the 'phase space' spanned by U and solutions of the differential equation are trajectories in this phase space. The first step consists in a study of the properties of the flow in the vicinity of its critical points U_* defined by $F(U_*) = 0$. These properties derive from the nature of the eigenvalues and eigenspaces of the tangent flow dF at U_*. The set of eigenvectors corresponding to eigenvalues with positive real part generates the subspace tangent to the so-called 'unstable manifold' denoted W_u. On the other hand, those corresponding to eigenvalues with strictly negative real part determine locally the 'stable manifold' denoted W_s. The critical point U_* attracts trajectories starting on its stable manifold for $t \to \infty$ and on the unstable manifold for $t \to -\infty$. It can happen that stable and unstable manifolds of U_* interesect somewhere else than at U_*. A case of special interest to us is when they intersect along a curve. Such a curve is called a 'homoclinic trajectory'. This situation is presented in figure 2 for a 2-dimensional vector field. Let λ_+ and λ_- be the two real eigenvalues (respectively positive and negative) of dF at U_*, which is here a 'hyperbolic point'. Along the homoclinic trajectory when $z \to \pm\infty$, $U \to U_*$, and behaves as $C_\pm \exp \lambda_\pm z$, where $C_\pm$ are the eigenvectors associated with $\lambda_\pm$. This special kind of trajectory is precisely what we are looking for to represent mathematically the physical 'solitary waves', since far from the region of strong deformation one recovers the unperturbed state. Similarly the solitary wave corresponding to a jump $h_1 \to h_2$ or $h_2 \to h_1$ should be described by 'heteroclinic trajectories' joining two different critical points. We now apply these general considerations to the flow defined by (7).

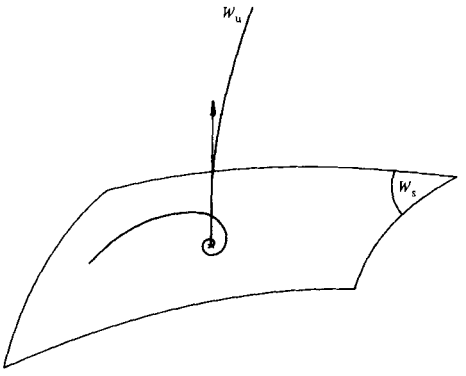

FIGURE 3. Local picture of phase space for the flow defined by (15) around the critical point $(1,0,0)$ for $v > 2$ and $R > R_c$. W_u and W_s are respectively the unstable and stable manifolds.

Critical points of (7) are given by $U_2 = U_3 = 0$ and the real roots of $(1-U_1)(U_1^2+U_1+1-\frac{3}{2}v) = 0$, that is to say $h_1 = 1$ and eventually h_2, the positive root of $U_1^2+U_1+1-\frac{3}{2}v = 0$ (the second, always negative, root of this equation is unphysical). At the critical point $U_*^{(1)} = h_1 = (1, 0, 0)$, the eigenvalues of the linearized flow are solutions of the equation

$$W\lambda^3+\tfrac{4}{5}(R-R_c)\lambda-\tfrac{3}{2}(v-2) = 0. \tag{9}$$

From this expression the sum of the 3 roots λ_i is zero. One is real, say λ_1, and has the sign of the product, i.e. of $v-2$. The other roots $\lambda_{2,3}$ may be real or complex-conjugate according to whether

$$4\left[\frac{4}{5W}(R-R_c)\right]^3+27\left[\frac{3}{2W}(v-2)\right]^2$$

is negative or positive. When $\lambda_{2,3}$ are real (respectively complex-conjugate) they (respectively their real part) have (has) the sign opposite to that of $v-2$. When $R > R_c$ the roots are always complex. When $v > 2$, λ_1 is positive and defines a 1-dimensional unstable manifold, the real part of $\lambda_{2,3}$ is negative and the stable manifold is 2-dimensional. The situation is depicted in figure 3. The physical consequence is that the front and the rear of a solitary wave are not symmetrical. At the front which corresponds to the limit $z \to +\infty$ the thickness of the film presents damped oscillations ($\lambda_{2,3}$ complex with negative real part), while at the rear the height relaxes to 1 without oscillations ($z \to -\infty$, λ_1 real and positive). This situation was observed by Kapitza & Kapitza (1949; see their plates (42) and (43)). When $v < 2$, we expect opposite results, i.e. a 1-dimensional stable manifold, a 2-dimensional unstable manifold, all arrows reversed in figure 3 and oscillations of the height at the rear and not at the front. Qualitatively we can understand this behaviour in noticing first that $v = 2$ is the velocity of infinitesimal perturbations at all wavevectors q; the velocity of any other perturbation has to be compared with this value, which presents itself as natural scale. Everything occurs as if a wave propagating quicker ($v > 2$) was pushing the surface ahead, inducing a buckling phenomenon (the oscillation of the thickness) analogous to the buckling of a plate under compression. The similarity also appears in the equations since the term $(R-R_c)/W$ in (11) is analogous to the load in the Föppl–von Kármán equations (see e.g. Landau & Lifshitz 1959*b*), both being proportional to a second-order derivative of the deviation while stabilizing effects are accounted for by fourth-order derivatives. Since on the rear the surface seems to be

dragged along by the wave it has no tendency to buckle and the thickness does not present oscillations. The case $v < 2$ is a mirror image of $v > 2$ since the wave moves more slowly than infinitesimal modes.

Stability properties of the other relevant critical point $U_*^{(2)} = (h_2, 0, 0)$ when it exists are also of interest. Eigenvalues of the tangent flow are the roots of

$$W\lambda^3 + \tfrac{4}{5}(R\eta_2^3 - R_c)\,\lambda - \frac{3}{2h_2^3}(v - 2h_2^2) = 0. \tag{10}$$

The analysis goes along parallel lines except that $v-2$ is replaced by $v-2h_2^2$. Using the equation which relates v to $h_1 = 1$ and h_2: $h_2^2 + h_2 + 1 - \frac{3}{2}v = 0$, we write

$$(2h_2^2 - v) + 2h_2 - v + 2 - v = 0,$$

and, assuming $v > 2$, we get $h_2 > 1$, and have

$$2h_2^2 - v > 2h_2 - v > 2 - v.$$

The last term being negative, the first term needs to be positive in order for the sum of the three terms to be equal to zero. Thus when $v > 2$, the critical point $U_*^{(2)}$ has a 2-dimensional unstable manifold and a 1-dimensional stable manifold which is the situation of $U_*^{(1)}$ when $v < 2$ and conversely.

Local analysis, even if it has already given a qualitative idea of the aspect of the solution corresponding to a homoclinic trajectory, is not enough to ascertain the existence of such solutions and their quantitative properties. To do this we must get a more global image of the flow $\mathrm{d}U/\mathrm{d}z = F(U)$ in phase space far from the critical points. This can be obtained by integrating the equations numerically, as shown in §3.2.

3.2. *Numerical search for solitary waves*

We can settle the problem of finding homoclinic trajectories as follows: a set of parameters R, B (or R_c), W being given, consider a sphere in phase space centred at the critical point $U_*^{(1)} = (1, 0, 0)$. If it is sufficiently small, for $v > 2$ the intersection of the 1-dimensional unstable manifold with this sphere will be a point P while the intersection of the 2-dimensional stable manifold will be a line L. A trajectory starting along the unstable manifold most often never comes back in the neighbourhood of $U_*^{(1)}$. However, for certain values of v it may approach it again. The corresponding trajectory will touch the sphere at a point Q. If it was an exact homoclinic trajectory, the trajectory would intersect the sphere at a point on L. Thus the rule of the game is to put Q on line L, which can be done by adjusting v. This will lead to a condition relating v to R, B and W. If Q does not belong to L the trajectory is only approximately homoclinic and the point in phase space is repelled from the vicinity of $U_*^{(1)}$ in the direction of the unstable manifold. The ideal homoclinic trajectory can only be approximated numerically. From a practical point of view we fix R and we look for v as follows: we define a function $d(v)$ which represents the minimum of the distance of 'first comeback' for a trajectory starting close to $U_*^{(1)}$ in the direction of the unstable manifold computed from (9). Integration of system (7) for trajectories far from being homoclinic diverges rapidly. For better chosen v, $d(v)$ can be defined unambiguously. The numerical value of v is further refined by dichotomy in order to make d as small as possible. This minimization process is slightly different from the one used to show that a relation should exist between v and the other parameter. In particular, it does not make reference to the stable manifold but a trajectory can come closer and closer to $U_*^{(1)}$ only if it comes closer and closer to the stable manifold, since otherwise it would be pushed away in the unstable direction. Anyhow, we never

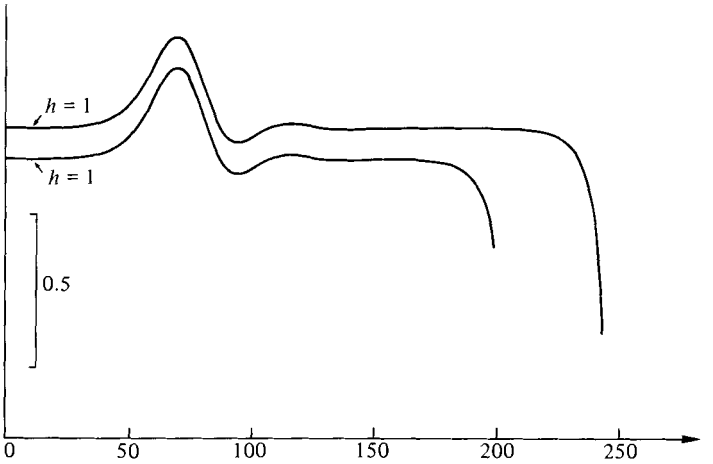

FIGURE 4. Example of determination of homoclinic trajectories of (15). We have plotted the height of the film as a function of x. The Reynolds number is $R = 10$. The distance between the critical point $(1, 0, 0)$ and the initial conditions is 10^{-4}. The shortest solution corresponds to $d(v) \lesssim 10^{-3}$ and $v = 2.4814328125$, while the other corresponds to $d(v) \lesssim 3 \times 10^{-4}$ and $v = 2.4814337890625$.

obtain an exact homoclinic trajectory but only approximate ones; however, our numerical results strongly suggest their existence: ultimately all numerical trajectories diverge, but, making more stringent the condition on the minimum of the distance $d(v)$ and choosing initial conditions as close as possible to $U_*^{(1)}$, we obtain trajectories which diverge at larger and larger values of z upon refinement of v (see figure 4 for an example).

In the (R, v) Cartesian plane, at B and W fixed (here $B = 5$ and $W = 3000$), the condition for homoclinic trajectories is split into several branches, each corresponding to one kind of solitary wave (figure 5). The different solitary waves are characterized by the number n of the principal humps (see figure 6 for $n = 2$). All these waves have a velocity larger than 2, and the different branches $v = v_n(R)$ corresponding to n-hump solutions all meet at $v = 2$ and $R = R_c = \frac{5}{4}B$. In the limit $R \to R_c^+$ and $v \to 2^+$ the solutions become infinitely extended and their amplitude vanishingly small. For $v < 2$, in order to keep a 1-dimensional unstable manifold we have integrated $\mathrm{d}\boldsymbol{U}/\mathrm{d}z = -F(\boldsymbol{U})$, which amounts to a change $z \to -z$, but we have found no homoclinic trajectories; we shall discuss this in more detail later. The last point worth noticing about figure 5 is the existence of a value R_n^* above which homoclinic trajectories with n humps no longer exist. R_n^* is an increasing function of n, and, on each upper branch when R decreases, the amplitude and velocity of every solution increase rapidly while the width of the perturbed region remains roughly constant.

3.3. *Analytical approach to some limiting cases*

In this section we analyse the behaviour of the solution at the two ends of the curves $v = v_n(R)$, that is to say in the limits $(R \to R_c;\ v \to 2)$ and $(R \to 0;\ v \to \infty)$.

Our numerical results show that for R close to R_c and small $v - 2$ the amplitude modulations in the solitary waves are small. In order to study this domain we assume $v = 2(1 + \epsilon)$ and $h = 1 + \epsilon\phi$, $\phi = O(1)$. That ϵ also scales h-variations is suggested by the fact that the distance between the two relevant critical points $U_*^{(1)}$ and $U_*^{(2)}$ along the $(U_1 \equiv h)$-direction is precisely ϵ at lowest order. When retaining the dominant terms, (6) reads, near $\epsilon = 0$,

$$W\phi''' + \tfrac{4}{5}(R - R_c)\phi' + 3\epsilon\phi(\phi - 1) = 0. \tag{11}$$

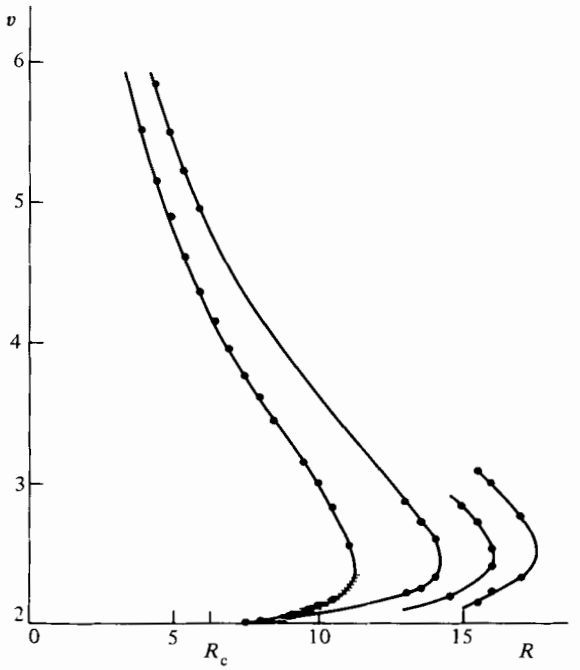

FIGURE 5. The values of the parameters (R, v) for which there exist homoclinic curves, W and R being fixed. The hatched branch contains the points which were actually observed in time-dependent simulations (cf. §4).

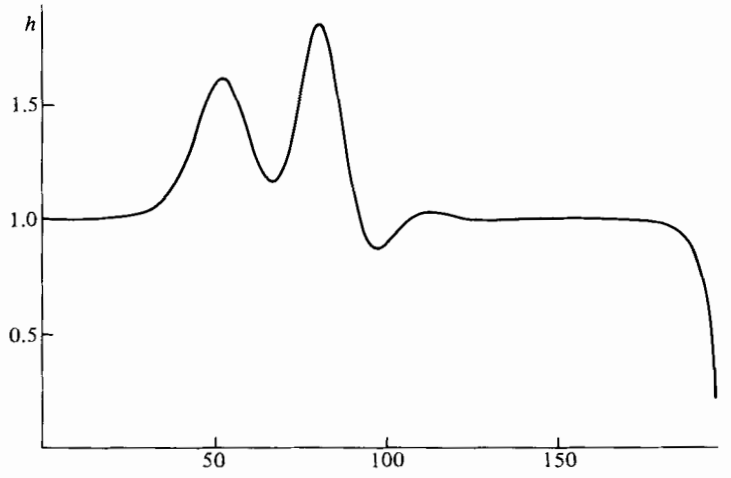

FIGURE 6. A homoclinic trajectory with two humps. This solution corresponds to the values of the parameter $R = 10$ and $v = 3.64$.

Solitary waves exist when a certain relation between R and v, here $R-R_c$ and ϵ, is fulfilled. In order to make this relation apparent we perform the variable change $z = \bar{z}(3\epsilon/W)^{\frac{1}{3}}$, obtaining

$$\phi''' + \mu\phi' + \phi(\phi - 1) = 0, \tag{12}$$

where the prime now denotes the derivative with respect to $\bar{z}$, and

$$\mu = \tfrac{4}{5}(9W)^{-\frac{1}{3}}\epsilon^{-\frac{2}{3}}(R - R_c). \tag{13}$$

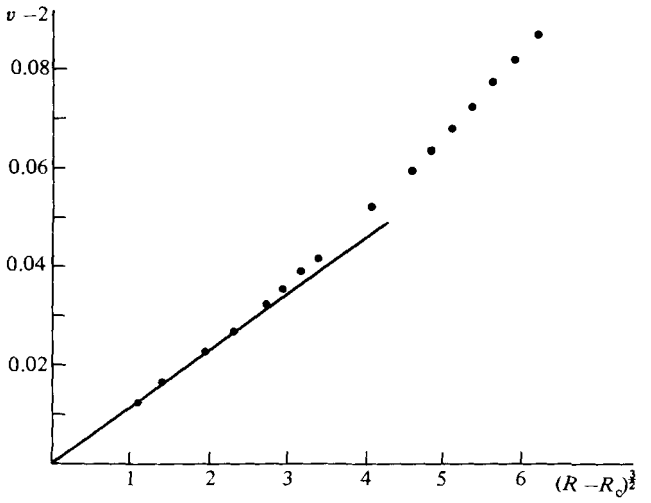

FIGURE 7. Behaviour of $v-2$ as a function of $(R-R_c)^{\frac{3}{2}}$ for small values of $R-R_c$ and $W = 3000$. The curve reaches the point $(v-2, (R-R_c)^{\frac{3}{2}}) = (0,0)$ with a finite slope, confirming the prediction of §3.3.

Since (12) depends only on the parameter μ, the existence of solitary waves is linked to special values of this parameter, say μ_n. Thus there exist families of homoclinic trajectories for (6) such that

$$\epsilon^{-\frac{2}{3}}(R-R_c) \sim \text{const} \quad \text{or} \quad (v-2) \sim (R-R_c)^{\frac{3}{2}}. \tag{14}$$

Although the numerical study becomes more and more difficult when $R-R_c$ tends to zero, it is in good agreement with the asymptotic behaviour predicted above (figure 7). *A posteriori*, this can be taken as a proof of the fact that ϵ also scales amplitude variations. At a local scale $U_*^{(1)}$ and $U_*^{(2)}$ have symmetrical properties, and this symmetry is present in (11), which does not enable us to understand why we have found homoclinic trajectories for $v > 2$ and not for $v < 2$. This shows quite clearly that the existence of homoclinic trajectories does not depend only on local properties but also on the global structure of the phase space.

This result can be compared with the other weakly nonlinear analyses. Since the correct scaling of z is $z \propto \bar{z}\epsilon^{\frac{1}{3}}$, the typical wavenumber of a solution is $\alpha \sim \epsilon^{\frac{1}{3}}$. Since $R-R_c \sim \epsilon^{\frac{2}{3}}$, we simply deduce that $R-R_c \sim \alpha^2$ on the branch of solitary waves.

If we relax the condition $v \sim 2$ and small amplitude there is no reason to forbid solutions for $R < R_c$, and from figure 5 we see that such solutions exist with $v \gg 2$, even for $R \to 0^+$ and a large amplitude. In order to obtain their asymptotic behaviour in the limit $R \to 0$, we have to return to (6). After division by h^3 it reads

$$\frac{h-1}{h^3}(h^2+h+1-\tfrac{3}{2}v) + (\tfrac{4}{5}Rh^3-B)h' + Wh''' = 0. \tag{15}$$

Integration of (15) over $(-\infty, +\infty)$ gives

$$\int \mathrm{d}z \frac{h-1}{h^3}(h^2+h+1-\tfrac{3}{2}v) = 0, \tag{16a}$$

and integration after multiplication by h' leads to

$$W\int \mathrm{d}z\, h''^2 = \int \mathrm{d}z\, (\tfrac{4}{5}Rh^3-B)h'^2. \tag{16b}$$

For the maximum $h_{\max}$ of the amplitude, we deduce from (16a, b) that, as orders of

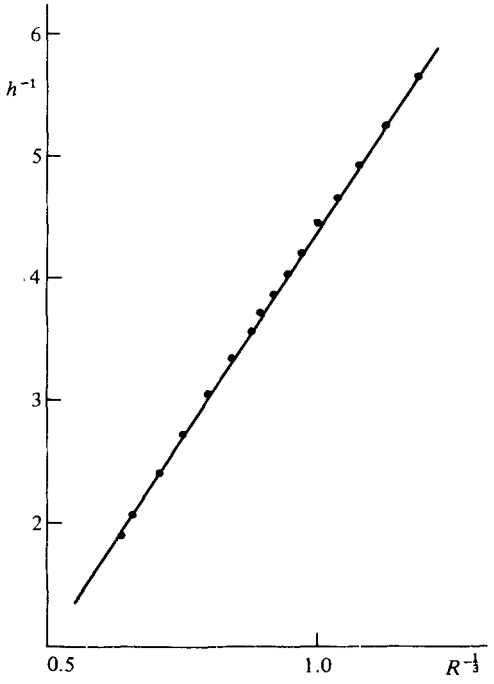

FIGURE 8

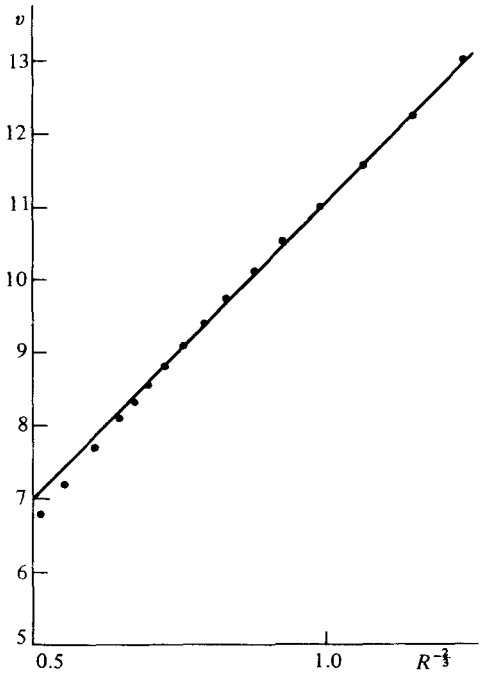

FIGURE 9

FIGURE 8. Behaviour of the amplitude of the localized one-hump solution as a function of $R^{-\frac{1}{3}}$, for $W = 3000$, $B = 5$.

FIGURE 9. The velocity of the localized solution as a function of $R^{-\frac{2}{3}}$, for $W = 3000$, $B = 5$.

magnitude: $Rh_{\max}^3 \sim$ const and $v \sim h_{\max}^2 \sim R^{-\frac{2}{3}}$. These asymptotic behaviours are in good agreement with our numerical results, as can be seen on figures 8 and 9, which display $h_{\max}$ and v as functions of $R^{-\frac{1}{3}}$ and $R^{-\frac{2}{3}}$ respectively.

3.4. *Additional remarks*

3.4.1. *On the existence of periodic or random wavetrains*

Solitary waves considered here are represented in a 3-dimensional phase space as homoclinic trajectories joining for $z \to \pm\infty$ a critical point with a 1-dimensional unstable manifold ($\lambda_1 > 0$) and a 2-dimensional stable manifold ($\lambda_{2,3} = \rho \pm i\omega$, $\rho < 0$) with $\lambda_1 + \rho > 0$. This situation has been considered from a mathematical point of view by Shil'nikov (1965, 1970), who showed that in the neighbourhood of the homoclinic trajectory there exists an infinity of periodic solutions (some results of Shil'nikov have been improved recently by Tresser 1981). The existence of these periodic solutions is crucial in understanding certain of our numerical results and also probably the large variety of solutions observed by Kapitza & Kapitza (1949). Qualitatively one can say that near the exact homoclinic trajectory there exist trajectories which closely resemble it for large portions but miss the critical point at the last moment, which gives birth to another almost homoclinic trajectory etc. An example of this case is given in figure 10, which displays a solution with two consecutive solitary waves – a solution which should not be confused with the 2-hump homoclinic curve given in figure 6. Periodically or randomly disposed almost-homoclinic curves can be obtained at will, which seem to correspond to certain regimes observed experimentally by Kapitza.

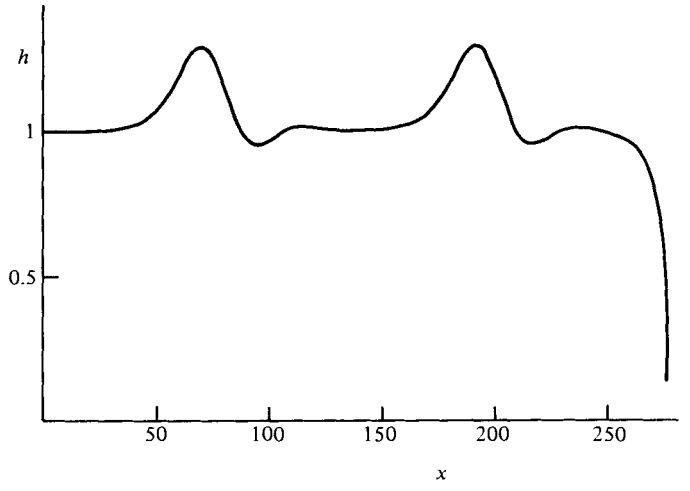

FIGURE 10. An example of an almost-homoclinic curve. These solutions give birth to wavetrains composed of solitary waves. The values of the parameters are $R = 11.26$ and $v = 2.481\,45$ ($W = 3000$ and $B = 5$).

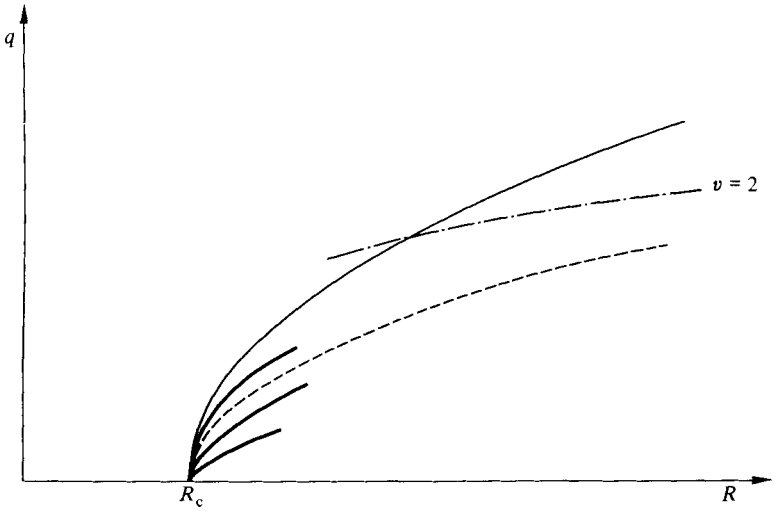

FIGURE 11. Comparison between weakly nonlinear analysis and our results: ——, neutral curve for linear analysis; —·—; curve of solutions for which $v = 2$; below this curve the velocities of the solution are greater than 2; - - - - -, curve of marginal stability for sideband mechanism; ——, branches of solitary waves.

As there exists a close connection between our solitary waves and periodic solutions it is possible to compare our weakly nonlinear results with the conclusions of Lin (1974) and Nakaya (1975) concerning the periodic waves. In the (R, α)-plane the curves of existence of solitary waves would correspond to $R - R_c \sim \alpha^2$. A possible situation is presented in figure 11.

Around these curves would exist a lot of periodic or almost-periodic waves. From our analytical approach we predict that their amplitude $\epsilon \propto \alpha^3$, which is in agreement with Nakaya's results, at least in the weakly nonlinear regime.

The absence of homoclinic trajectories for $v < 2$ can also be related to the weakly

nonlinear analysis. The existence of a whole domain around (R_c, $q = 0$) in which the velocity of solutions, determined in a perturbative expansion, is greater than 2 is in agreement with our findings (see figure 11).

3.4.2 *Heteroclinic trajectories and hydraulic jumps*

Besides homoclinic trajectories we can also find heteroclinic trajectories, that is to say trajectories joining two different critical points. As already shown for $v > 2$, in addition to $U_*^{(1)} = (1, 0, 0)$ we have to consider $U_*^{(2)} = (h_2, 0, 0)$, where h_2 is the positive root of $h^2 + h + 1 - \frac{3}{2}v = 0$ ($h_2 > 1$). The stable manifold of this critical point is 1-dimensional (it is a curve in the ordinary sense) while its unstable manifold is 2-dimensional (a surface). Since two surfaces intersect along a line in 3-dimensional space, in general this unstable manifold will intersect the 2-dimensional stable manifold of the other critical point $U_*^{(1)}$. The heteroclinic trajectory is a solution leaving $U_*^{(2)}$ along its unstable manifold and reaching $U_*^{(1)}$ along its stable manifold. Such solutions correspond to a jump with a height h_2 upstream and 1 downstream. Owing to the imaginary parts of the eigenvalues the height h oscillates both at the head and the rear of the jump. Such solutions can be obtained numerically either directly as before or by using the methods developed in §4 (see especially §4.1.1). The reverse case of a heteroclinic trajectory going from $U_*^{(1)}$ to $U_*^{(2)}$ should be quite exceptional, since it corresponds to a reconnection of two 1-dimensional manifolds in 3-dimensional space. This remark allows us to understand the global lack of symmetry between $U_*^{(1)}$ and $U_*^{(2)}$ in phase space and gives a clue to the reason why which we have not found homoclinic trajectories for $v < 2$. Indeed what seems important to the structure of phase space is the existence and relative positions of points $U_*^{(1)}$ and $U_*^{(2)}$. We have seen that, when $v > 2$, then $h_2 > h_1 = 1$, and one could find either homoclinic trajectories starting from $U_*^{(1)}$ and coming back to $U_*^{(1)}$ or heteroclinic trajectories starting from $U_*^{(2)}$ and going to $U_*^{(1)}$ while no $U_*^{(2)} \to U_*^{(2)}$ or $U_*^{(1)} \to U_*^{(2)}$ trajectories could be found. When $v < 2$ the roles of $U_*^{(1)}$ and $U_*^{(2)}$ are inverted and we expect opposite results, i.e. the possibility of homoclinic trajectories $U_*^{(2)} \to U_*^{(2)}$ and heteroclinic ones $U_*^{(1)} \to U_*^{(2)}$ but not the reverse. This is a global property of phase space not accessible to local analysis. Note that the convention plays a part in labelling the critical point. An integration constant K being given, the structure of the phase space is fixed by v and K. And we may define h_1 and h_2 as the two real positive roots of $h^3 - \frac{3}{2}vh = K$ with the supplementary convention $h_1 < h_2$. Then we can draw a definite global picture of phase space. The identification of one of the values h_1 or h_2 as the physical unperturbed height is not mathematically relevant even if it controls the nature of possible trajectories.

3.4.3 *On the role of the order of the gradient expansion*

This discussion seems to invoke the dimension of phase space in a crucial way. However, the existence of a relation between the parameters R, B, W and v is related to the very nature of the problem. Let us suppose that in our gradient expansion we had considered terms up to the nth order. The phase space for the flow $\mathrm{d}U/\mathrm{d}z = f(U)$ would be n-dimensional. To determine homoclinic trajectories we demand that an m-dimensional manifold (the stable manifold of the critical point U^*) intersects an $(n-m)$-dimensional manifold (the unstable manifold of U^*) along a curve. This leads precisely to a relation between R, W, v and B. It is more difficult to see, from a general point of view, that the shape of the surface, up- and downstream from the perturbed region, would be unchanged by such a modification of the equations, since the critical elements of U^* are changed.

3.4.4. *Choice of numerical values*

To fulfil the conditions of validity of the long-wavelength expansion leading to (3), we chose large values of W ($W = 1000$ and 3000) and a finite value of B ($B = 5$). With these choices we sought a condition between R and v for the existence of homoclinic trajectories for (8). We have actually performed numerical calculations with other values of W and B, nominally of order unity. This avoided the formal manipulation of large numbers by the computer. This was compatible with the basic assumption of our model, owing to the following remark. Let us make the (formal) change of length- and timescales $\bar{x} = kx$, $\bar{t} = kt$ in (3). It becomes

$$h_{\bar{t}} + (\tfrac{2}{3}h^3 + (\tfrac{8}{15}kRh^6 - \tfrac{2}{3}kBh^3)\, h_{\bar{x}} + \tfrac{2}{3}Wk^3h^3h_{\bar{x}\bar{x}\bar{x}})_{\bar{x}} = 0. \tag{3'}$$

The problem with $W = 1000$ (or 3000) and $b = 5$ is thus equivalent to a new problem with $\bar{W} = k^3W$, $\bar{B} = kB$, $\bar{R} = kR$, up to this change of length and time limit. Let l (respectively $\bar{l}$) be the typical size of the solution of (3) (respectively (3')) extrapolated from the numerical results with $W = 1000$ (respectively $\bar{W} = 1000k^3$), $B = 5$ (respectively $\bar{B} = 5k$) and R (respectively $\bar{R} = kR$). Consistency with the initial assumption demands $Wl^{-2} \sim 1$ and $l^{-1} \ll 1$. In terms of $\bar{W}$ and $\bar{l}$, these conditions read $\bar{W}\bar{l}^{-2} \sim k$ and $\bar{l} \gg k$. For a matter of convenience, we have chosen $k = 0.1$. All our numerical results satisfy the previous conditions, showing that they are indeed consistent with the formal expansion sketched in §1.

4. Numerical study of the initial-value problem

The existence of a special class of solutions which are stationary in a moving reference frame is not the only point to consider. We have also tried to investigate their relevance. This is a difficult question which relates first to the stability of these solutions and second to the way in which they attract initial conditions taken in the complete (x, t)-domain. A theoretical approach to this problem is difficult. In this section we present a partial answer (of experimental nature) given by the numerical simulation of the initial-value problem for the complete equation (3). The simulation takes place on a finite domain $0 < x < L$ with various boundary conditions at $x = 0$ and L. At time $t = 0$ we choose an initial condition localized in space; that is to say one that differs from a constant only on a small interval (x_1, x_2), the perturbation being smooth and sufficiently small. To generate the time evolution, we used a finite-difference scheme which is quasilinearized and implicit of the Crank–Nicholson type (see e.g. Richtmyer & Morton 1967); the lattice spacing $\Delta x = 0.125$ and time step $\Delta t = 0.125$ are small enough to give sufficient accuracy. This can be controlled by checking that $\int_0^L h(x,t)\,\mathrm{d}x$ is constant in time – a property which derives directly from (3) for periodic boundary conditions and which also holds as long as the localized solutuion does not interact with boundaries in the other cases. If Δx and Δt are too large, the discrete analogue of $\int_0^L h(x,t)\,\mathrm{d}x$ drifts slowly.

4.1. *Numerical results with non-periodic boundary conditions*

4.1.1. *Heteroclinic trajectories*

Let us begin with results obtained on the jump corresponding to the heteroclinic trajectory $U_*^{(2)} \to U_*^{(1)}$. For this simulation we assumed $h_x = h_{xx} = 0$ at $x = 0$ and $x = L$. The initial condition was a step from h_2 at $x = 0$ to h_1 at $x = L$, $h_2 > h_1$ (= 1

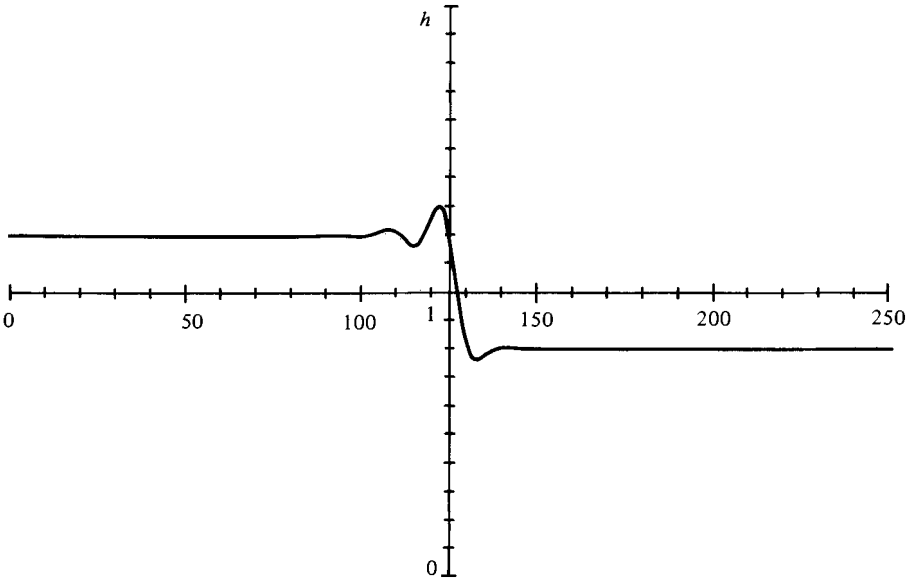

FIGURE 12. A steady hydraulic-jump solution of (10). One observes a buckling phenomenon both up- and downstream of the perturbed region.

eventually) localized at $x = \frac{1}{2}L$ and smoothed by a cosine arc. The simulation was performed in a frame moving at the velocity $v = \frac{2}{3}(h_1^2 + h_1 h_2 + h_2^2)$ deduced from the previous analysis. For R small enough the wave is steady in that frame and has the expected profile (see figure 12). However, when R increases we observed a time-dependent buckling (see figure 13), and, for even larger R, h can become negative after some time so that the solution loses its physical meaning.

4.1.2. *Homoclinic trajectories*

We now turn to the homoclinic trajectories. Using the same boundary conditions and initial conditions with $h_1 = h_2 = 1$ and a small 'cosine-bell' bump at $x = \frac{1}{2}L$, we observe the formation of a solitary wave very similar to those obtained in §3. Figure 14 displays such a solution. However, it is very difficult to choose the velocity v of the reference frame in order to observe a steady solution. If v is not properly chosen the solution slowly moves in one or the other direction, and interactions with one of the boundaries cannot be neglected after a while. In order to avoid this difficulty and to follow a solution over arbitrarily long times, we have performed simulations with periodic boundary conditions. The main conclusion of this subsection is that solitary waves as studied in §3 exist effectively in the sense that they attract a non-void set of initial conditions in the (x, t)-domain. The question of their long-term stability is the subject of §4.2.

4.2. *Long-term evolution of waves*

4.2.1. *Numerical results with periodic boundary conditions*

Here we present the numerical solutions obtained for $L = 125$, $W = 1000$ and $B = 5$, the maximum of the amplitude of the initial perturbation being 0.005.

(i) For $R < R_c$ the initial perturbation is damped more and more slowly as $R \to R_c$. At large times the solution tends to the basic one $h \equiv 1$.

(ii) For $R > R_c$ the initial perturbation grows and changes its shape to resemble homoclinic solutions with 1 hump calculated in §3. This first evolution is the same

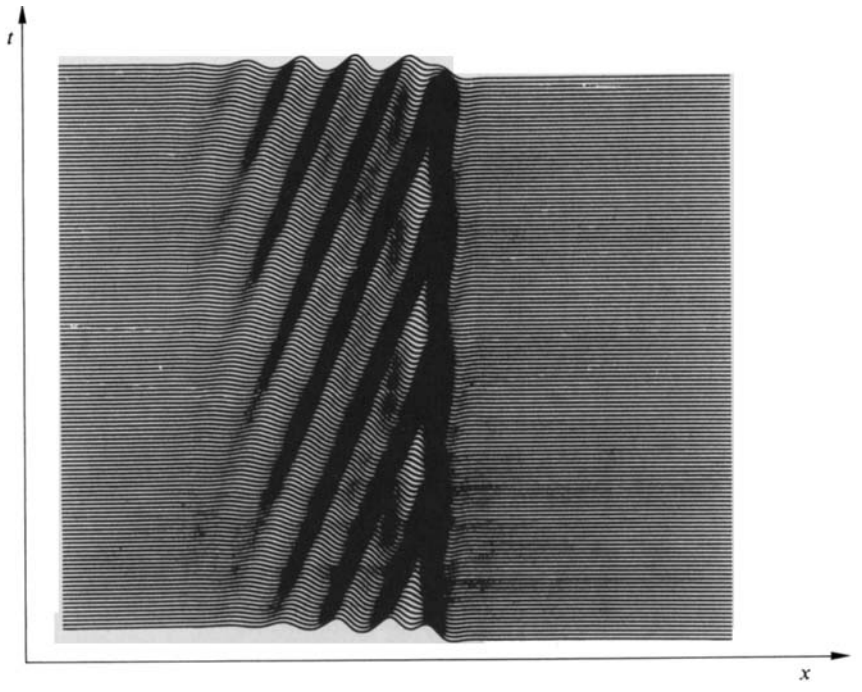

FIGURE 13. Evolution of an hydraulic jump as a function of time. The time-dependent buckling of the free surface only appears beyond a given value of the Reynolds number. Two successive curves are separated by a time interval $\Delta t = 20$.

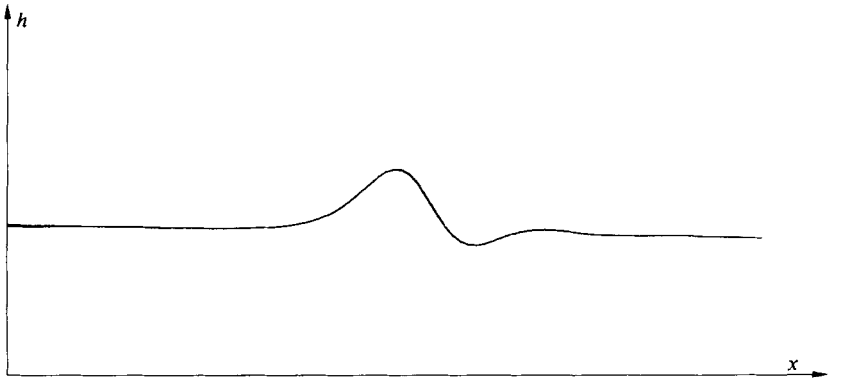

FIGURE 14. A solitary wave stationary in a reference frame. This solution was observed imposing $h_x = h_{xx} = 0$ at the boundaries.

as what was seen with boundary conditions $h_x = h_{xx} = 0$ (§4.1.2); however, we are now able to follow the solution over longer periods of time and to observe new features. The first point to mention is the growth of a wavetrain at the tail of the main perturbation which keeps advancing with an almost constant shape. This wavetrain is made of a small number of oscillations with a small amplitude. It remains localized in space while advancing at a lower speed (it seems to move back with respect to the reference frame moving at $v = 2$). When this train is sufficiently far from the main solitary wave, the process repeats itself. Since we are dealing with periodic boundary conditions, the perturbation collides with the slowest ones. This

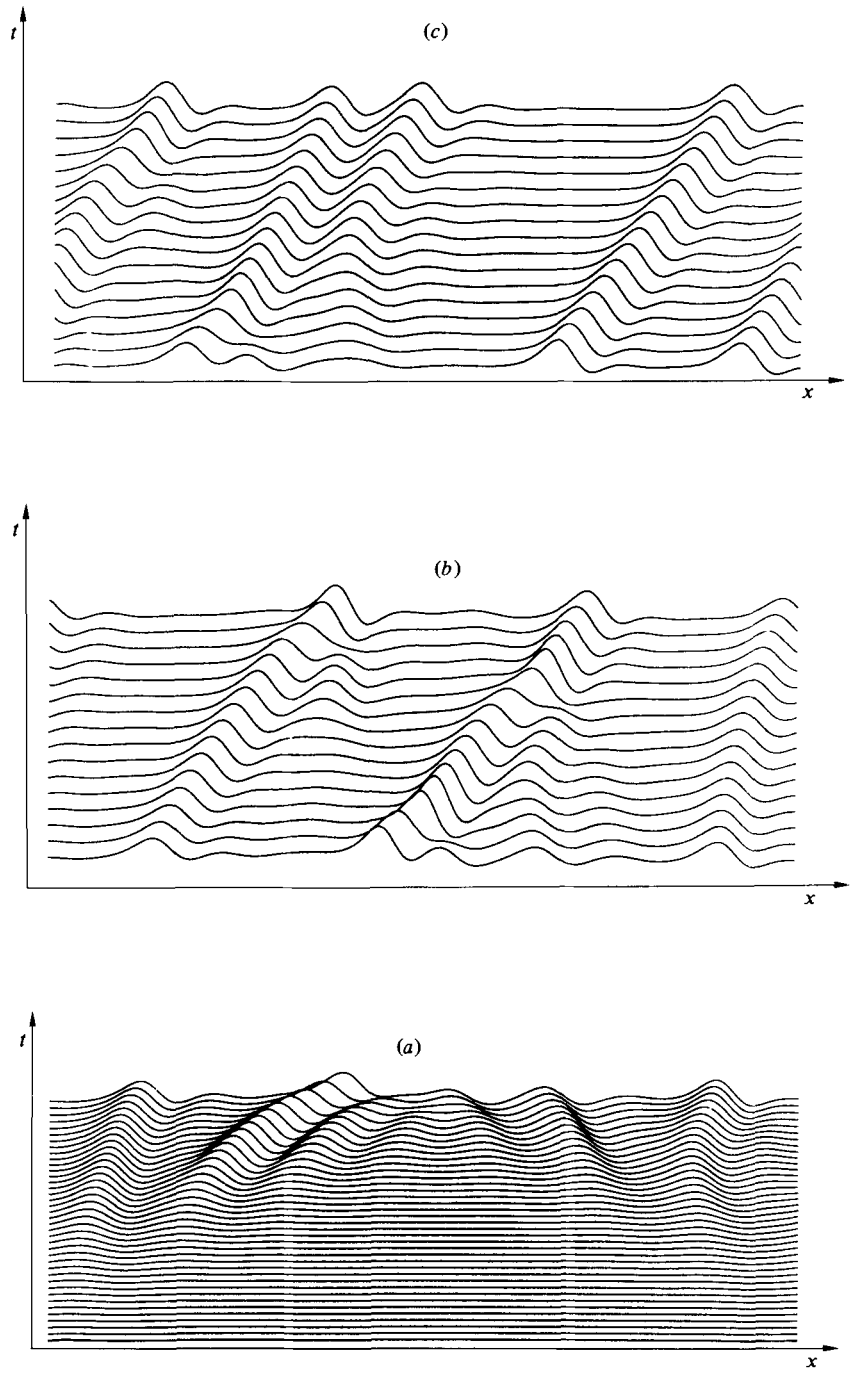

FIGURE 15. Evolution of the solution in a large box ($L = 125$), with periodic boundary conditions. (*a*) The growth of the initial localized perturbation and the appearance of a complicated shape of the surface. (*b*) The final stage of an interaction between two localized perturbations. (*c*) A collision between two solitary waves. These figures were obtained for the values $R = 9$, $W = 1000$, $B = 5$. The frame in which the equations were studied is moving at velocity $v = 2$, and the time interval between two curves is $\Delta t = 250$.

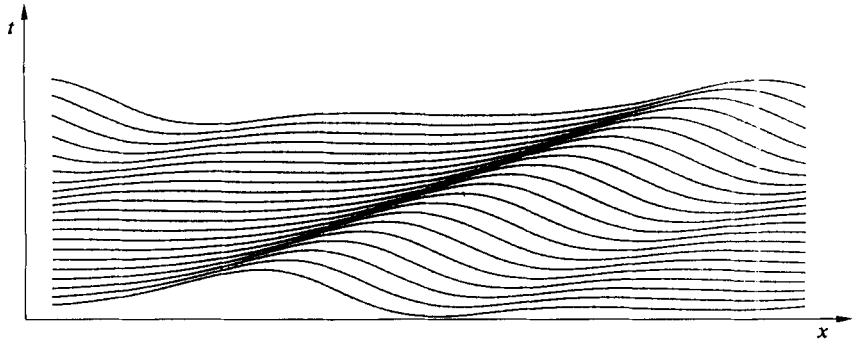

FIGURE 16. Regular solitary waves obtained in a small box with periodic boundary conditions, and with the values of the parameters $R = 9$, $W = 1000$, $B = 5$. Time lapse between two successive curves is $\Delta t = 100$.

collision changes drastically the shape of the surface for a while, but the solution recovers a remarkably localized aspect a short time after the collision. In fact we observe a rather disordered regime during a very long time, the solution being composed of several solitary waves in interaction (see figure 14). The nature of this disorder – turbulent or not – will be discussed in §4.2.2. It seems that the solution tends towards a regular arrangement of solitary waves. This is suggested by the result of the simulation over a much smaller length presented in figure 16 ($L = 25$).

(iii) The situation depicted above holds as long as R is smaller than a certain value R^* above which catastrophic events occur. R^* is obviously related to the critical value R_1^* above which no 1-hump solitary wave exists; however, we have not tried to check this numerically. When $R > R^*$ the beginning of the evolution is the same as before, but after a finite time lapse the main perturbation gains a large amplitude and starts to evolve quickly, all derivatives becoming large. The numerical solution remains finite, however, owing to the strong stability of the implicit numerical scheme, but from one space step to the next variations are very large, and the numerical results lose any connection with the partial differential equation. This phenomenon remains unchanged when the resolution is increased by a factor of two; moreover it happens nearly at the same instant with the same initial condition. This is an indication that this catastrophic evolution is a property of the equation for $R > R^*$ independently of the numerical integration scheme.

(iv) We make the following remarks. (*a*) This 'catastrophic' behaviour occurs for all R if the amplitude of the initial perturbation is too large. (*b*) We have not succeeded in growing waves with more than 1 principal hump like that of figure 6. Whenever 1-hump solutions are possible, they seem to mask the other kinds of wave which have a much smaller amplitude, and, when 1-hump solutions are no longer possible, it is likely that solutions with several humps do not attract a large set of initial conditions. (*c*) Solitary waves with large amplitude and large velocity corresponding to the upper parts of the branches in figure 5 have never appeared. The reason is either the preceding one or more probably that they are intrinsically unstable.

4.2.2. *Existence and stability of waves*

The simulations presented above undoubtedly confirm that there exist solitary waves of the kind derived using the dynamical-systems approach. But only the simplest kind seems easily producible, and even in that case we observe unexpected features: wavetrains at the rear of a solitary wave, and an apparently disordered regime when several solitary waves interact. The first problem mentioned can find

an explanation from the instability of the basic flow for $R > R_c$ against fluctuations with wavevector around $q_{max} = [\frac{2}{5}(R-R_c)/W]^{\frac{1}{2}}$ which corresponds to the most unstable mode. A similar phenomenon has already been invoked for localized solutions of (17) below (Kuramoto & Tsuzuki 1976).

We consider the second problem in two steps. First we examine whether the evolution is turbulent or not, concluding that it is not and next we interpret this evolution as a diffusive relaxation towards some final state.

From figure 15 one can think that the motion has become random due to the chaotic interaction of waves. There is also a second reason to suspect weak turbulence: using a limit different from ours, Sivashinsky & Michelson (1980) and later Sivashinsky & Shlang (1982) have shown that the evolution of the fluid film could be reduced to that of a variable ϕ governed by the equation

$$\partial_t \phi + \phi \partial_x \phi + \partial_{xx} \phi + \partial_{xxxx} \phi = 0. \tag{17}$$

This equation appears in several contexts (chemical oscillations, chemically reacting fronts and flames. . .) and it is known to have spontaneously turbulent solutions for L sufficiently large. However, in accordance with a referee's suggestion, this does not imply that a turbulent film is the only consequence. It may imply that the three-dimensional character of waves becomes important in some parameter range. The stabilizing effect of the additional dimension was discussed by Krishna & Lin (1977).

In order to characterize numerically the character – turbulent or not – of a solution of a dynamical system, one determines its Lyapunov numbers (see e.g. Benettin, Galgani & Strelcyn 1976). These numbers relate to the stability of the given trajectory in phase space. When they are all non-positive, errors do not grow exponentially, and the trajectory is stable. When some Lyapunov numbers are positive errors are exponentially amplified and the trajectory is unstable. The system is sensitive to initial conditions and becomes unpredictable in the long term: i.e. it is turbulent (Ruelle 1978). Once discretized in space, partial differential equations such as (3) or (17) can be considered a a system of N coupled ordinary differential equations – the degrees of freedom being the values of h at the N points of the lattice – and Lyapunov numbers can be computed – Ruelle (1980) proved in some cases the existence of a discrete spectrum of Lyapunov numbers for infinite-dimensional dynamical systems, which may be considered as an extension of partial differential equations.

Irregular solutions of (17) for large enough L do have positive Lyapunov numbers, the number of which increases linearly with L (Pumir 1982), but in the present problem the largest Lyapunov number actually tends to zero as time goes on; the irregular evolution of waves cannot be considered as turbulent but seems to correspond to slow relaxation towards a steady regime. The latest state of this relaxation can be understood as a diffusive process. In order to show this, we first remark that (3) is autonomous so that its solutions are invariant under time–space translations and infinitesimal perturbations corresponding to this invariance property are neutral. Consequently we expect that the latest perturbations to relax will be close to these neutral modes. In order to study this final evolution we adapt to the present problem the formalism devised to deal with perturbations linked to the position or 'phase' of the cell pattern in convection (see e.g. Eckhaus 1965; Benjamin 1967; Benjamin & Feir 1967). Assume that h_f is the final solution travelling at speed v: $h_f(x,t) = h_f(z = x - vt)$. Owing to translational invariance, $h_f(z+\phi)$ is also a solution as long as ϕ is a constant 'phase'. If we allow for slow variations of ϕ, i.e. ϕ slowly varying with z and t, then $h_f(z+\phi)$ is no longer a solution, and corrections to it have

to be calculated. We look for h in the form: $h(z,t) = h_f(z+\phi(z,t)) + \delta h$ and replace $h_f(z+\phi)$ by its Taylor series:

$$h(z,t) = h_f(z) + \phi(z,t)\, h_f'(z) + \tfrac{1}{2}\phi^2 h_f''(z) + \ldots + \delta h^{(1)} + \delta h^{(2)} + \ldots, \tag{18}$$

where we assume that $\delta h^{(i)}$ is of the order of the ith derivative of ϕ with respect to z or t (z-derivative on h_f are denoted by primes). In the moving frame, (3) reads

$$\mathrm{L}[h] \equiv (\partial_t - v\,\partial_z)\, h + \partial_z(\tfrac{2}{3}h^3 + \tfrac{8}{15}(Rh^6 - E_c\, h^3)\,\partial_z h + \tfrac{2}{3}Wh^3\,\partial_z^3 h) = 0 \tag{19}$$

and inserting h in this equation one gets a hierarchy of linear problems of the form

$$\Lambda \delta h^{(i)} = M^{(i)} \quad (i = 1, 2, \ldots), \tag{20}$$

where Λ is obtained from L by linearization around h_f. The linear operator Λ has a non-trivial kernel h_f', since, for ϕ = const and small,

$$\mathrm{L}[h_f(z+\phi)] = \mathrm{L}[h_f(z) + \phi h_f'(z)] = \mathrm{L}[h_f(z)] + \phi \Lambda h_f' \equiv 0. \tag{21}$$

Thus equations of the form (20) will have a solution only if they satisfy a solvability condition of the form

$$(\tilde{h}, M^{(i)}) = 0,$$

where $\tilde{h}$ belongs to the (non-void) adjoint kernel of Λ (it satisfies $\Lambda^+ \tilde{h} = 0$) Λ being the adjoint of Λ^+ in the sense of some inner product defined on the same interval as $h(z)$. The dynamics of ϕ will be defined order after order through these solvability conditions. At first order we get

$$\Lambda \delta h^{(1)} = -A(z)\,\partial_z \phi - B(z)\,\partial_t \phi, \tag{22}$$

where $A(z)$ and $B(z)$ are easily obtained upon substitution. This existence condition reads $A\,\partial_z \phi + B\,\partial_t \phi = 0$, where $A = (\tilde{h}, A(z))$ and $B = (\tilde{h}, B(z))$ are some constants *a priori* different from zero, but which we shall not attempt to calculate. The qualitative content of this order is that an infinitesimal phase perturbation propagates at a well-defined velocity $v' = -A/B$. Equation (30) can be solved assuming $\delta h^{(1)} = \partial_z \phi a_1$, which gives $\Lambda a_1 = (AB(z) - BA(z))/B$. To go to next order it is convenient to change from the (z,t) reference frame to the $(z' = z - v't,\ t' = t)$ reference frame in which the perturbation is steady at this order. Going to next order (∂_z^2 or $\partial_{z'}^2$) this perturbation is no longer steady, but just relaxes according to a diffusion law $\partial_{t'}\phi = D\partial_{z'}^2 \phi$, where the diffusion coefficient D expresses itself as the ratio of two scalar products in the same way as v' does. This 'phase diffusion' or sideband (in)stability is not limited to the domain of weak nonlinearities. As shown by Pomeau & Manneville (1979), this exists for periodic steady solutions of translationally invariant equations describing irreversible processes. Thus there is no immediate connection between our considerations, concerning the fully nonlinear domain, and the properties related to Eckhaus-like instabilities, which refer usually to the weakly nonlinear domain, where analytic results can be more easily obtained.

In the weakly nonlinear domain we can compare our results with Lin's (1974) predictions. Both approaches are compatible if one of the curves of figure 11 is above the line of neutral stability with respect to the sideband mechanism while the other curves (corresponding to more than one hump) are below. It would be very difficult to go beyond this formal approach in order to obtain the explicit values of v' and D (this would require knowledge of the final solution and it would be necessary to determine the kernel of the adjoint to Λ before calculating the scalar products). However, even at this level one is able to understand the final evolution of the

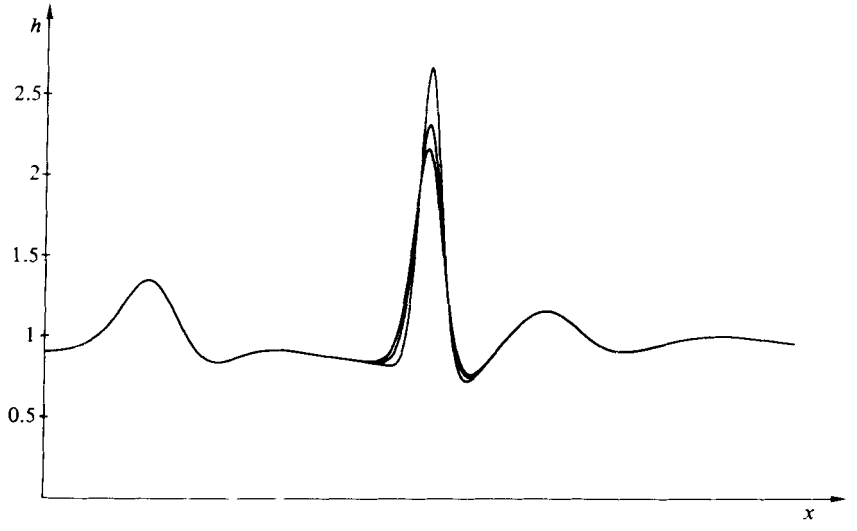

FIGURE 17. Final stage of catastrophic evolution. The shapes of the surface at three different times separated by $\Delta t = 0.4$ are superposed. The maximum of the solution grows very quickly and the perturbed region becomes narrower and narrower. Numerical values of the parameters are $R = 13$, $W = 1000$ and $B = 5$.

solution. The sign of D determines the stability of the solution against compression-/dilatation modes. If D were negative the solution would be unstable – in cellular convection this would be the Eckhaus instability (Eckhaus 1965). Here 'experimentally' for $R < R_*$ one has a true relaxation and $D > 0$. The fluctuations are damped in the moving frame (z', t'). In a box of length L the slowest relaxing mode has the wavenumber $q = 2\pi/L$ and the relaxation rate is $1/\tau = D(2\pi/L)^2$. For $L = 25$ we have estimated τ to be of the order of 400, which is pretty long. For $L = 125$ the steady state will be much more difficult to reach (see figure 15), and for $L \to \infty$ an algebraic relaxation $\sim t^{-\frac{1}{2}}$ is expected as usual for diffusive processes.

To end this section let us come back to the catastrophic behaviour observed when the amplitude of the perturbation is too large (e.g. for $R > R^*$). Figure 17 displays the superposition of 3 successive time steps immediately before the moment when the numerical solution loses its meaning as a solution of the partial differential equation. We can observe a narrowing of the perturbed region and a rapid increase of the amplitude. This leads to think that the solution has a singularity at some finite time t_0 ($= 0$ for convenience). This suggests that we look for this catastrophic solution under the form of a superposition $h = h_{\text{reg}} + h_{\text{sing}}$ where the regular part remains finite and smooth. The singular part will be taken as

$$h_{\text{sing}} = |t|^{-\alpha} H(x|t|^{-\beta}), \tag{23}$$

where α and β should be positive in order to reproduce the numerical features. Replacing h in (3), setting $X = xt^{-\beta}$, and keeping the most-divergent terms we get $\alpha = \frac{1}{9}$, $\beta = \frac{1}{6}$, and, with the change $H \to (\frac{25}{32}W/R^2)^{\frac{1}{6}} H$, $x \to (\frac{5}{2}W^2/R)^{\frac{1}{6}} x$, a universal equation for H is obtained:

$$-\left(\tfrac{1}{3}H + \tfrac{1}{2}X\frac{\mathrm{d}H}{\mathrm{d}X}\right) + \frac{\mathrm{d}}{\mathrm{d}X}\left[H^5\frac{\mathrm{d}H}{\mathrm{d}X} + H^3\frac{\mathrm{d}^3H}{\mathrm{d}X^3}\right] = 0, \tag{24}$$

together with the boundary conditions $H \to 0$ when $X \to \pm\infty$, since the singular part contributes only in the vicinity of the singularity. We will not attempt to solve this

equation, but the fact that one can find an equation for the scaling function H with positive α and β corroborates well the numerical evidence. However, the initial conditions leading to such an evolution remain unknown. The existence of this singularity can be interpreted physically as a breaking of the film, but notice that derivatives become large just before this breaking so that the weak gradient assumptions needed in the derivation of (3) are no longer fulfilled. Notice also that a breaking of the film with appearance of a contact line could happen if $h = 0$ somewhere. Writing (3) in the form

$$\partial_t\left(\frac{1}{h}\right) = P(h, h_x, h_{xx}, h_{xxx}, h_{xxxx})$$

(where P is a polynomial) shows that h cannot reach zero as long as $h, \ldots, h_{xxxx}$ are not singular.

5. Summary and conclusion

In this paper we have studied the nonlinear evolution of waves at the surface of a fluid film flowing down an inclined plane. The starting point is a nonlinear partial differential equation derived under the following assumptions: (i) the restriction to 2-dimensional flow; and (ii) slow variations in the direction of the flow when compared with variations through the thickness of the film.

Above a certain critical Reynolds number R_c the flat film is unstable against small waves running at twice the fluid velocity at the surface ($v = 2$). Weakly nonlinear analysis in terms of the amplitude equation shows that the bifurcation is supercritical: i.e. the bifurcated state is stable for $R > R_c$ and its amplitude goes to zero when $R \to R_c^+$. Here we wanted to give up the reference to delocalized periodic waves and to tackle the full nonlinear problem for localized perturbations in order to see whether such finite-amplitude perturbations could trigger a subcritical instability. We looked for localized waves in assuming the existence of solutions steady in a moving reference frame. This leads to a formulation in terms of ordinary differential equations and to the identification of these waves with 'homoclinic trajectories' in phase space. The net result was a relation between the velocity v of the wave and the Reynolds number R. The most noticeable points were (i) the absence of localized waves with velocity $v < 2$; (ii) the existence of different types of waves according to the number of principal humps; (iii) the existence of a maximum value R_n^* above which n-hump solutions disappear; and (iv) the existence of waves with $R < R_c$ and a large amplitude. This study was completed by numerical simulations of the initial-value problem intended to check the physical relevance of these results. It turned out that, during the evolution, the only kind of wave that could be recognized was related to the 1-hump solution corresponding to the lower branch of the curve $v(R)$. Moreover, the initial-value problem has a solution for all times and sufficiently small perturbation only if $R < R_*$, the catastrophic behaviour observed for $R > R_*$ probably being related to a singularity at a finite time for the solution of the partial differential equation. We observed neither solutions with more than one hump over long enough durations nor solutions corresponding to the upper branches of $v(R)$ (large amplitude, large velocity). Finally all solutions observed corresponded to $R > R_c$. The basic state $h = \text{const}$ being unstable against infinitesimal periodic perturbations, this instability leads to the formation of growing wave-packets on the tail of a solitary wave, and at a later stage to trains of solitary waves. The evolution was complicated but definitely not turbulent, with some evidence of a slow relaxation of diffusive type.

All the results summarized above may help to understand qualitatively the great variety of flow regimes observed experimentally by Kapitza & Kapitza. In particular, the stability analysis of critical points of the associated dynamical system and the subsequent qualitative description of homoclinic trajectories suggest an explanation for the profile of the waves, while the simulation reproduces the generation of wavetrains and their organization. An obvious limitation of our analysis is the assumption of a 2-dimensional flow. Indeed, if a wave appears one should test its stability against distortions in the plane of the flow but in the direction transverse to the motion; i.e. undulations of the wave front in amplitude or phase (position). Such distortions would be coupled with velocity changes so that a truly chaotic regime could emerge, as observed for example by Binnie (1957) or Tably & Portalsky (1962). There could also exist localized perturbations (i.e. disturbances confined in a finite region of the inclined plane). The difficulty in introducing a third coordinate comes from the fact that the finite-dimensional dynamical-system theory has to be abandoned, but an approximate theory keeping only few Galerkin modes could perhaps allow for an understanding of the basic couplings leading to chaos. A similar remark should hold for the problem of birth and growth of localized structures in the process of intermittent transition to turbulence in pipes.

REFERENCES

Benettin, G., Galgani, L. & Strelcyn, J. M. 1976 Kolmogorov entropy and numerical experiments. *Phys. Rev.* **A14**, 2338–2345.

Benney, D. J. 1966 Long waves in liquid film. *J. Maths & Phys.* **45**, 150–155.

Benjamin, T. B. 1957 Wave formation in laminar flow down an inclined plane. *J. Fluid Mech.* **2**, 554–574.

Benjamin, T. B. 1967 The instability of periodic wave trains in certain nonlinear systems. *Proc. R. Soc. Lond.* **A299**, 59–75.

Benjamin, T. B. & Feir, J. E. 1967 The disintegration of wave trains on deep water. *J. Fluid Mech.* **31**, 209–249.

Binnie, A. M. 1957 Experiments on the onset of wave formation on a film of water flowing down a vertical plane. *J. Fluid Mech.* **2**, 551.

Eckhaus, W. 1965 *Studies in Nonlinear Stability Theory.* Springer.

Gjevik, B. 1970 Occurrence of finite amplitude surface waves on falling liquid films. *Phys. Fluids* **13**, 1918–1925.

Kapitza, P. L. & Kapitza, S. P. 1965 Wave flow of thin layers of a viscous fluid. In *Collected Works*, pp. 690–709. Pergamon.

Krishna, M. V. G. & Lin, S. P. 1977 Non-linear stability of a viscous film with respect to three-dimensional side-band disturbances. *Phys. Fluids* **20**, 1039–1044.

Kuramoto, Y. & Tsuzuki, T. T. 1976 Persistent propagation of concentration waves in dissipative media far from thermal equilibrium. *Prog. Theor. Phys.* **55**, 356.

Landau, L. D. & Lifshitz, E. M. 1959*a* *Fluid Mechanics.* Pergamon.

Landau, L. D. & Lifshitz, E. M. 1959*b* *Theory of Elasticity.* Pergamon.

Lin, S. P. 1969 Finite-amplitude stability of a parallel flow with a free surface. *J. Fluid Mech.* **36**, 113–126.

Lin, S. P. 1974 Finite-amplitude side-band instability of a viscous film. *J. Fluid Mech.* **63**, 417–429.

Nakaya, C. 1975 Long waves on a thin fluid layer flowing down an inclined plane. *Phys. Fluids* **18**, 1407–1412.

Pomeau, Y. & Manneville P. 1979 Stability and fluctuations of a spatially periodic convection flow. *J. de Phys. Lett.* **40**, 1609–1612.

Pumir, A. 1982 Thèse 3ème cycle, Université de Paris VI.

Richtmyer, R. D. & Morton, K. W. 1967 *Difference Methods for Initial Value Problems.* Wiley-Interscience.

RUELLE, D. 1978 Sensitive dependence on initial condition and turbulent behavior of dynamical systems. *Ann. NY Acad. Sci.*, 408–416.

RUELLE, D. 1980 Characteristic exponents and invariant manifolds in Hilbert space. *IHES Preprint.*

SHIL'NIKOV, L. P. 1965 *Sov. Mat. Dokl.* **6**, 163.

SHIL'NIKOV, L. P. 1970 *Mat. USSR Sb.* **10**, 91.

SIVASHINSKY, G. I. & MICHELSON, D. M. 1980 On irregular wavy flow of a liquid film down a vertical plane. *Prog. Theor. Phys.* **63**, 2112–2114.

SIVASHINSKY, G. I. & SHLANG, T. 1982 Irregular flow of a liquid film down a vertical column. *J. de Phys.* (Paris) **43**, 459–466.

SMALE, S. 1967 Differentiable dynamical systems. *Bull. AMS* **73**, 747.

SWINNEY, H. L. & GOLLUB, J. P. (eds) 1981 *Hydrodynamic Instabilities and the Transition to Turbulence.* Springer.

TABLY, S. R. & PORTALSKY, S. 1962 The determination of the wavelength on a vertical film of liquid flowing down a hydrodynamically smooth plate. *Trans. Inst. Chem. Engrs* **40**, 114–122.

TRESSER, C. 1982 On some theorems of L. P. Shil'nikov and some applications (to be published).

TRITTON, D. J. 1977 *Physical Fluid Dynamics.* Van Nostrand.

YIH, C. S. 1963 Stability of liquid flow down an inclined plane. *Phys. Fluids* **6**, 321–334.